UCRL- 84341
PREPRINT
CONF-800551--5

Status of (n, Charged Particle) Measurements at LLL

Robert C. Haight
and
Steven M. Grimes

This paper was prepared for submittal to

Symposium on Neutron Cross Sections from 10 to 50 MeV
Long Island NY
May 12-14, 1980

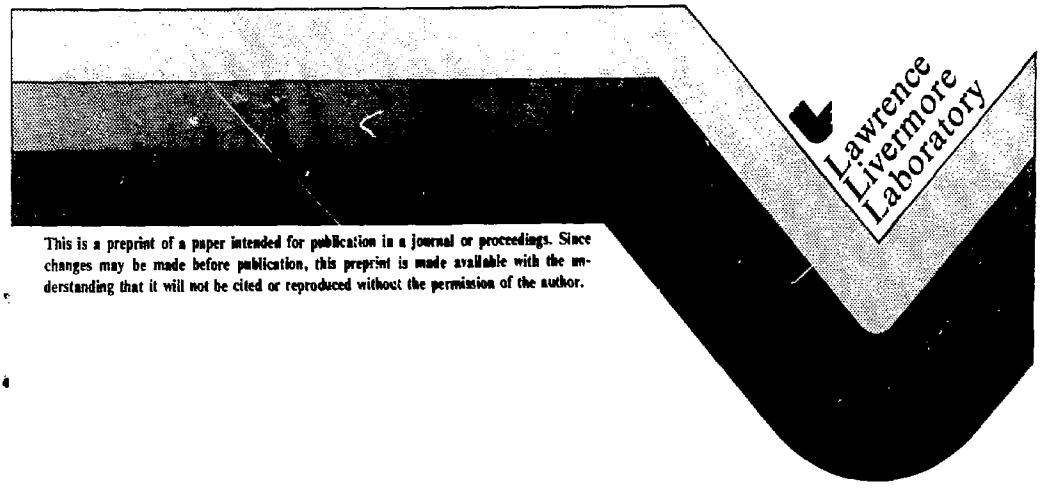

STATUS OF (N, CHARGED PARTICLE) MEASUREMENTS AT LLL*

Robert C. Haight and Steven M. Grimes†

Lawrence Livermore Laboratory
Livermore, California 94550 U.S.A.

ABSTRACT

Using a charged-particle magnetic-quadrupole spectrometer, we have studied (n, charged particle) reactions on materials bombarded with 14- to 15-MeV neutrons. Charged-particle production cross sections, angular distributions and spectra are measured. The materials investigated to date include most of those proposed for fusion reactor structures, Al, Ti, Cr, V, Fe, Ni, Cu, Nb and stainless steels 304 and 316. Isotopic data on ^{46,48}Ti, ^{50,52}Cr, ^{54,56}Fe, ^{58,60}Ni and ^{63,65}Cu and on the monoisotopic elements ^{27}Al, ^{51}V and ^{93}Nb have provided stringent tests of reaction model calculations. Equilibrium and pre-equilibrium reaction mechanisms have been identified and quantified. Preliminary data on ^{92,94,95,96}Mo and on light nuclides including ^{12}C and ^{7}Li have been obtained recently.

INTRODUCTION

Charged-particle producing reactions of neutrons with materials are of great importance in the development of fusion power. These reactions lead to the production of hydrogen and helium which can alter significantly the properties of materials. These reactions are responsible for a large part of the energy deposited locally in many materials by the neutrons. Nuclear transmutation results from these reactions since the product nucleus is always that of a different element than the target. Finally, cross sections of interest in neutron transport and in displacement damage can be obtained from the study of these reactions.

For the past four years a study of (n, charged particle) reactions has been underway at Livermore with a magnetic quadrupole

---

†Work performed with J. D. Anderson (LLL) and K. R. Alvar, H. H. Barschall and R. R. Borchers (Univ. of Wisconsin).

spectrometer. An earlier report on the development of this spectrometer was given in the preceeding symposium [1]. The spectrometer has undergone further development since then and a wide range of measurements has been completed while others are currently in progress. This report is of the present status of the program.

EXPERIMENTAL DEVELOPMENTS

The magnetic quadrupole spectrometer has previously been described [1,2]. Briefly, the spectrometer consists of a reaction chamber containing the samples which are irradiated with an intense 14-MeV neutron flux, a magnetic quadrupole triplet lens to transport the charged particles, and a ΔE-E detector system. The magnetic lens, which focusses the particles from the target foil onto the detectors, allows the detectors to be moved several meters (typically 2.5 m in our experiments) from the neutron source. The source at the same time can be quite close (5 to 10 cm) to the target foil. The result is a high neutron flux at the foil and a low background at the detectors because of the $1/r^2$ factor and the additional shielding that can be used. The solid angles for detecting charged particles does vary with charged-particle energy at a given magnet setting and several magnet settings must be used to cover the entire spectral range (Fig. 1).

Developments since the last symposium include larger detectors to increase the solid angle, thin-window proportional counters for use as a ΔE detectors for lower energy particles, a helium gas cell for normalization of the low energy alpha spectra, and a specially shaped neutron-production target to allow study of the reactions at 14 MeV. These developments were spurred by the desires to increase the sensitivity of the spectrometer, to be able to investigate more thoroughly low energy charged particles from light nuclei, and to eliminate the variation of neutron energy with reaction angle.

The typical E detector used now is a 300 mm^2 1500 μm silicon surface barrier detector. This thickness is chosen to stop the most energetic protons, 15 MeV, that we expect to produce with 14-15 MeV neutrons. It should be noted that intrinsic Ge detectors of larger area have recently been used at Ohio University [3].

The ΔE detector now in use is a two-element proportional counter filled with 96% Ar-4% CO_2. Its entrance window is several layers (≈ 5) of formvar supported by .025 mm tungsten wires spaced .13 mm apart. This combination can sustain a pressure of at least 8 kPa (60 mm of Hg) over a 1" active diameter. The design of the window is similar to that of ref. 4. Alpha particles to 700 keV have been detected with the ΔE_1-ΔE_2-E coincidence at 9 mm gas pressure.

The high pressure helium gas cell [5] was required to normalize the low energy alpha-particle production cross sections where the detector efficiency is not easily determined from the measured efficiencies for protons or deuterons. A "known" spectrum of

alpha particles is produced by n-α elastic scattering in the helium which is thick enough to stop the alpha particles that would traverse the length of the cell. We calculate the known spectrum from the stopping powers and then deduce the system efficiency by comparing the calculation with the measured spectrum at each magnet setting.

To produce 14-MeV neutrons with our facility, a neutron production angle of 90° is required. Previously this angle was not accessible with the rotating target since the 90° direction was tangential to the locally spherical surface and the neutrons needed to pass through several centimeters of copper before reaching the target. A truncated, conically-shaped rotating target now allows the samples to be placed in the 90° neutron production plane so that measurements can be done at the fusion neutron energy of 14 MeV.

UPDATED RESULTS

A spectrum of protons emitted at 90° from 15-MeV bombardment of ^{58}Ni [6] is shown in Figure 2 to illustrate the range and quality of the data. By integrating such spectra over energy and angle, we arrive at the total proton, deuteron and alpha-particle production cross sections of Table I [6-9]. Average charged-particle energies are also given in the table.

The total hydrogen and helium production cross sections, depicted in Figure 3, show large variations from element to element. It must be remembered however that the responses of materials to the hydrogen and helium produced will certainly be different. With these data and those from other sources, the assessment of materials for fusion application can now be based on a cross section set that is reliable at the 14-MeV fusion neutron energy.

MODEL INTERPRETATION

Model calculations are essential to provide much of the neutron cross section data base, in particular where experimental data are not sufficient. The extrapolation of the cross sections to energies not yet investigated is an example of where a calculational model is necessary.

The spectral and angular distribution data, as well as the cross sections, obtained with the magnetic quadrupole spectrometer provide especially stringent tests of the models. From our results we are able to test the validity of equilibrium and pre-equilibrium particle emission models.

Equilibrium Particle Emission

At 14-MeV incident neutron energy, the open reaction channels usually include (n,p), (n,n'p), (n,pn), (n,d), (n,α), (n,n'α) and other one or two light-particle-emission modes. For nearly all of

the nuclei listed in Table I, the preponderance of proton and alpha-particle emission is well described by emission from an excited nucleus at thermodynamic equilibrium in the first as well as successive stages. Both the spectral shapes (Fig. 4) and angular distributions (Fig. 5) give evidence for this reaction mechanism.

The importance of second-chance proton emission from (n,n'p) can vary widely with isotope as illustrated in Fig. 6 for ^{46}Ti and ^{48}Ti. Because of the relationship between neutron and proton separation energies, there is a region of excitation of ^{46}Ti that can decay by proton emission with no competition to neutron emission. This region accounts for the large, wide peak in the proton emission spectrum just above 2 MeV. A comparable region in ^{48}Ti does not exist and the second chance proton emission peak is nearly absent. This effect is explained also quantitatively [7].

Pre-Equilibrium Particle Emission

Evidence for pre-equilibrium proton and alpha-particle emission is also clear from the spectra (Fig. 7) and angular distributions (Fig. 5). The model used is the hybrid model of Blann [10] and reasonable agreements with the angle-integrated data are found. An interpretation of the angular distributions is qualitative so far in that the pre-equilibrium particles are expected to go mostly in forward directions. A more quantitative analysis remains a challenge.

From the present data, we can conclude generally that the fractional contribution of pre-equilibrium processes increases with a decreasing equilibrium component. Within an element, the pre-equilibrium component is usually more significant for the heavier isotopes.

PRESENT AND FUTURE WORK

Recent preliminary data have been obtained for ^{92,94,95,96}Mo, C and ^{7}Li. A spectrum of protons emitted at 90° from ^{94}Mo bombarded with 15-MeV neutrons is shown in Figure 8 for example.

Measuring the complete spectrum of charged particles from light isotopes poses experimental difficulties because particles of very low energy must be detected. For ^{12}C for example the (n,n'3α) reaction yields most of the alpha particles but with an average energy of only about 2 MeV. We have preliminary data showing that at many angles, the alpha particle spectrum is significant even below 1 MeV. This situation is expected also in the ^{7}Li (n,n'αt) and ^{16}O(n,n'4α) reactions, both of which are of importance for fusion applications.

In the future we plan to complete the measurements on the light nuclides, ^{7}Li, ^{9}Be, ^{11}B, ^{12}C, ^{14}N, ^{16}O and ^{19}F at E_n = 14 MeV; to extend the measurements on structural materials to Zr and others; and, using the LLL cyclograaff facility as a neutron source, to investigate the energy dependence of the cross sections.

ACKNOWLEDGMENTS

*Work performed under the auspices of the U.S. Department of Energy by Lawrence Livermore Laboratory under contract no. W-7405-ENG-48.

REFERENCES

1. S. M. Grimes, R. C. Haight, J. D. Anderson, K. R. Alvar, and R. R. Borchers, Symposium on Neutron Cross Sections from 10 to 40 MeV, ed. M. R. Bhat and S. Pearlstein, Brookhaven National Laboratory report BNL-NCS-50681 (1977), pp 297-304.

2. K. R. Alvar, H. H. Barschall, R. R. Borchers, S. M. Grimes and R. C. Haight, Nucl. Instr. and Meth. 148, 303 (1978).

3. G. Randers-Pehrson, R. W. Finlay, P. Grabmayer, V. Kulkarni, R. O. Lane, and J. Rapaport, this Symposium.

4. R. G. Markham, S. M. Austin, and H. Laumer, Nucl. Instr. and Meth. 129, 141 (1975).

5. R. C. Haight, C. Rambo, J. Cormier and J. Garibaldi, Nucl. Instr. and Meth. 164, 613 (1979).

6. S. M. Grimes, R. C. Haight, K. R. Alvar, H. H. Barschall, and R. R. Borchers, Phys. Rev. C19, 2127 (1979).

7. S. M. Grimes, R. C. Haight, and J. D. Anderson, Nucl. Sci. Eng. 62, 187 (1977).

8. R. C. Haight, S. M. Grimes, and J. D. Anderson, Nucl. Sci. Eng. 63, 200 (1977).

9. S. M. Grimes, R. C. Haight, and J. D. Anderson, Phys. Rev. C17, 508 (1978).

10. M. Blann, Phys. Rev. Lett. 27, 337 (1971); Nucl. Phys. A213, 570 (1973).

TABLE I

Proton, deuteron and alpha-particle emission cross sections and average charged-particle energy

Target	Particle Emitted	Cross Section (mb)	Spectrum-Averaged Charged-Particle Energy (MeV)
^{50}Cr	p	830 ± 100	4.5 ± 0.2
^{50}Cr	d	12 ± 4	5.6 ± 0.6
^{50}Cr	α	94 ± 15	8.4 ± 0.3
^{52}Cr	p	180 ± 25	4.7 ± 0.2
^{52}Cr	d	8 ± 3	4.9 ± 0.7
^{52}Cr	α	36 ± 6	8.4 ± 0.4
Cr	p	180 ± 25	4.7 ± 0.2
Cr	d	10 ± 3	5.7 ± 0.7
Cr	α	38 ± 6	8.6 ± 0.4
^{54}Fe	p	900 ± 110	4.8 ± 0.2
^{54}Fe	d	10 ± 4	5.6 ± 0.6
^{54}Fe	α	79 ± 13	8.7 ± 0.4
^{56}Fe	p	190 ± 22	5.1 ± 0.2
^{56}Fe	d	8 ± 3	5.5 ± 0.7
^{56}Fe	α	41 ± 7	8.8 ± 0.6
Fe	p	230 ± 30	5.0 ± 0.2
Fe	d	8 ± 3	5.4 ± 0.8
Fe	α	43 ± 7	8.8 ± 0.4

TABLE I (Cont'd)

Target	Particle Emitted	Cross Section (mb)	Spectrum-Averaged Charged-Particle Energy (MeV)
^{58}Ni	p	1000 ± 120	5.1 ± 0.2
^{58}Ni	d	14 ± 6	6.5 ± 0.7
^{58}Ni	α	106 ± 17	9.5 ± 0.3
^{60}Ni	p	325 ± 40	5.0 ± 0.2
^{60}Ni	d	11 ± 4	6.0 ± 0.8
^{60}Ni	α	76 ± 12	9.0 ± 0.3
Ni	p	790 ± 100	4.9 ± 0.2
Ni	d	13 ± 5	6.3 ± 0.6
Ni	α	97 ± 16	9.2 ± 0.4
^{63}Cu	p	320 ± 45	4.4 ± 0.2
^{63}Cu	d	9 ± 4	6.4 ± 0.7
^{63}Cu	α	56 ± 10	8.9 ± 0.3
^{65}Cu	p	44 ± 5	6.2 ± 0.3
^{65}Cu	d	10 ± 4	6.6 ± 0.8
^{65}Cu	α	13 ± 3	9.5 ± 0.7
Cu	p	237 ± 28[a]	5.0 ± 0.3[a]
Cu	d	10 ± 4[a]	6.5 ± 0.8[a]
Cu	α	42 ± 7[a]	9.1 ± 0.4[a]

[a]Inferred from isotopic data.

Figure 1. Measured transmissions of protons for nine magnet current settings with 50 mm^2 ΔE and E detectors. The transmissions are expressed as effective solid angles for detecting protons emitted from the target foil. Approximately nine settings are required to cover the proton energy spectra for the structural elements, Al to Nb.

Figure 2. Proton emission cross sections at 90° for natural nickel bombarded with 15-MeV neutrons.

Figure 3. Hydrogen and helium production cross sections at 15 MeV measured with the magnetic-quadrupole charged-particle spectrometer.

Figure 4. Spectrum of alpha particles from $^{50,52}Cr$, $^{54,56}Fe$, $^{58,60}Ni$ and $^{63,65}Cu$ bombarded with 15-MeV neutrons. The solid curves are Hauser-Feshbach calculations. The dashed curves indicate the alpha spectrum from the first stage of the reactions.

Figure 5. Variation with angle of the cross sections for emission of protons, deuterons, and alpha particles from the bombardment of ^{50}Cr with 14.8 MeV neutrons. The cross sections are normalized to unity at 30°.

Figure 6. Proton-emission spectra from ^{46}Ti and ^{48}Ti bombarded with 15-MeV neutrons. The large bump in the spectrum for ^{46}Ti near 2 MeV is due to protons from (n,n'p) reactions which are favored for this isotope but not for ^{48}Ti. This effect originates in the relationship of neutron to proton separation energies and has been called "proton trapping" or "second chance proton emission."

Figure 7. High energy portions of the proton emission cross sections are compared with hybrid model calculations (dot-dashed line), multistep Hauser-Feshbach calculations (dashed line) and the sum of these contributions (solid line).

Figure 8. Preliminary data for protons emitted at 90° from ^{94}Mo bombarded with 15-MeV neutrons.

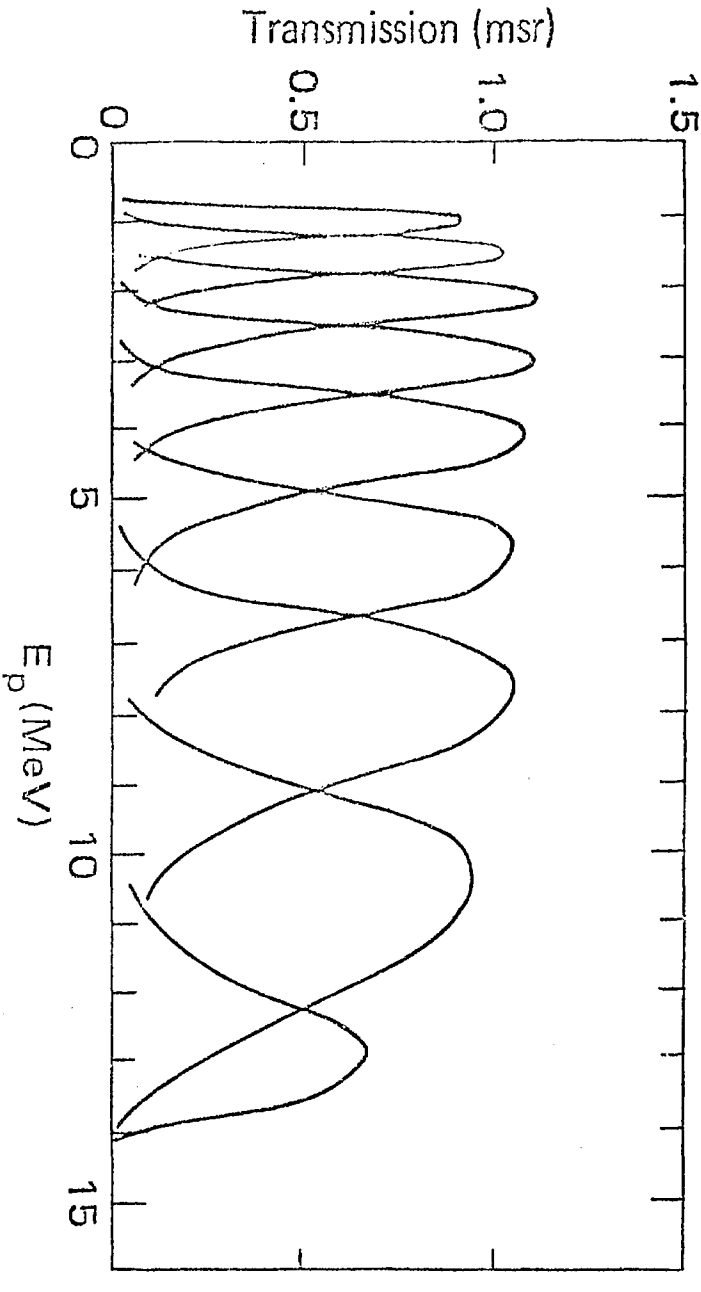

Figure 1

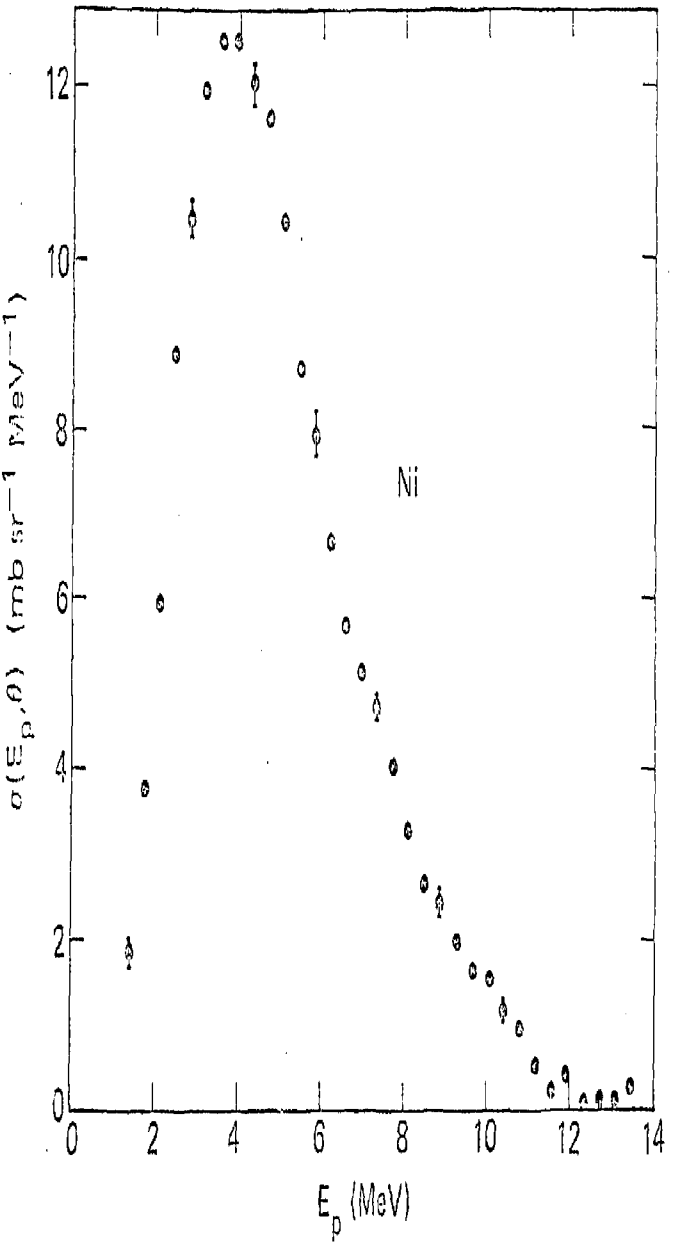

Figure 2

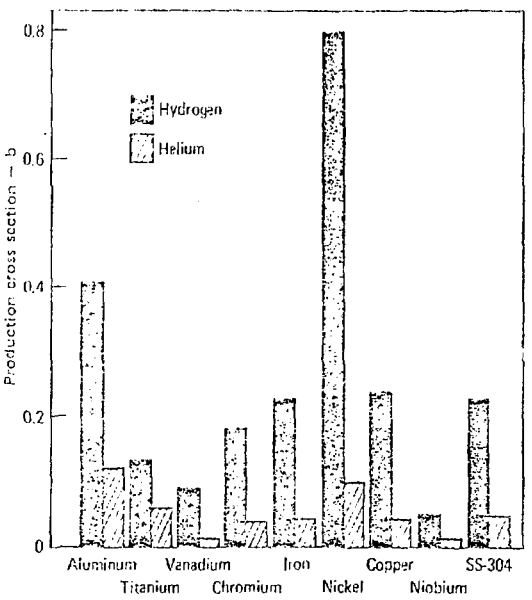
0.8
0.6
0.4
0.2
0
Production cross section — b
Hydrogen
Helium
Aluminum
Titanium
Vanadium
Chromium
Iron
Nickel
Copper
Niobium
SS-304

Figure 3

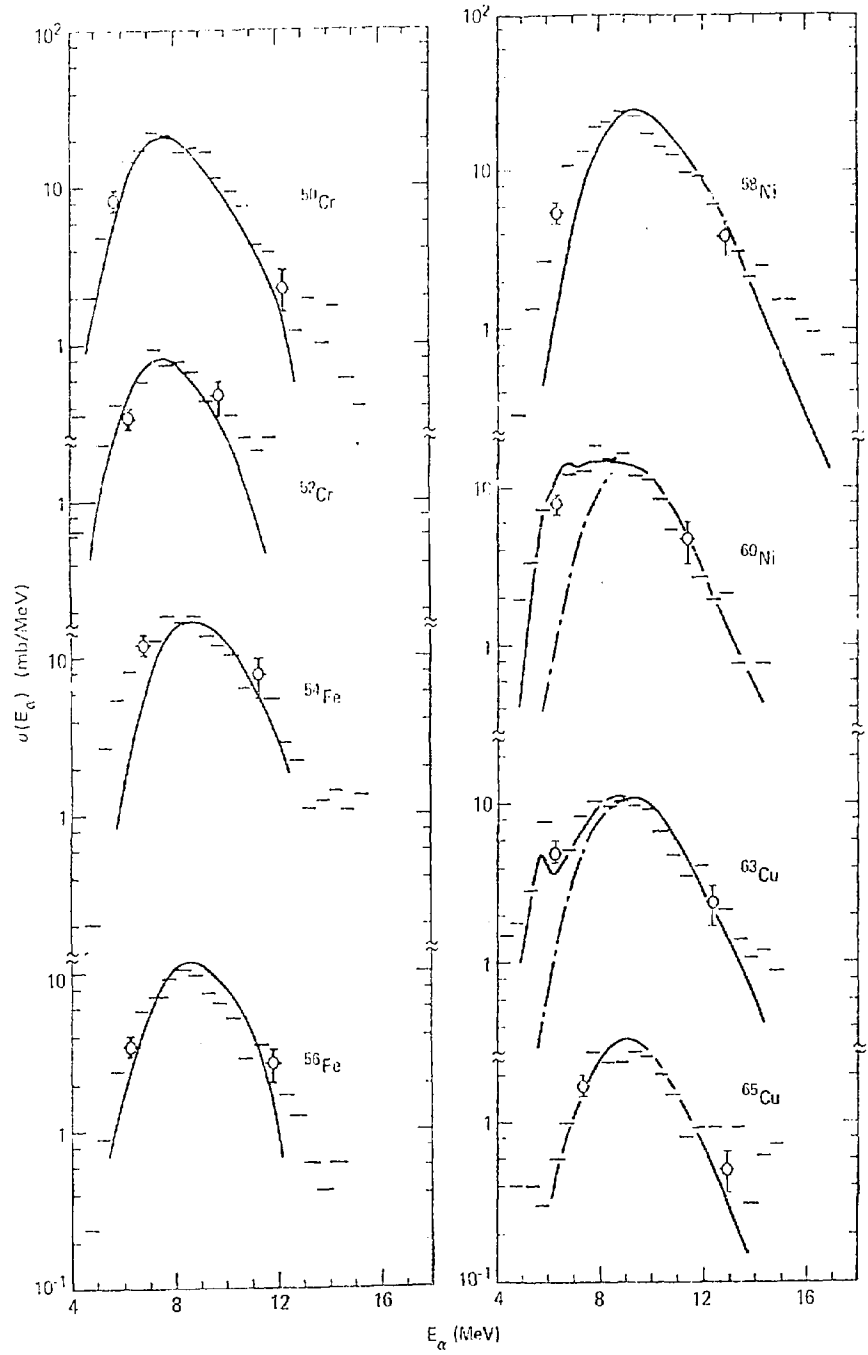
10^2
10
1
10^{-1}
^{50}Cr
^{52}Cr
^{54}Fe
^{56}Fe
^{58}Ni
^{60}Ni
^{63}Cu
^{65}Cu
4
8
12
16
$\sigma(E_\alpha)$ (mb/MeV)
E_α (MeV)

Figure 4

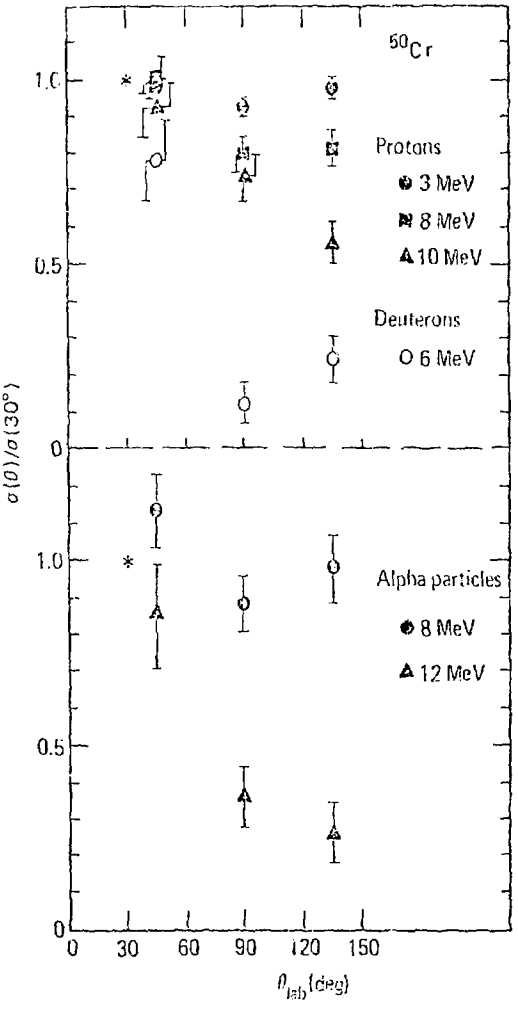
^{50}Cr
Protons
3 MeV
8 MeV
10 MeV
Deuterons
6 MeV
Alpha particles
8 MeV
12 MeV
1.0
0.5
0
1.0
0.5
0
0
30
60
90
120
150
$\sigma(\theta)/\sigma(30°)$
θ_{lab}(deg)

Figure 5

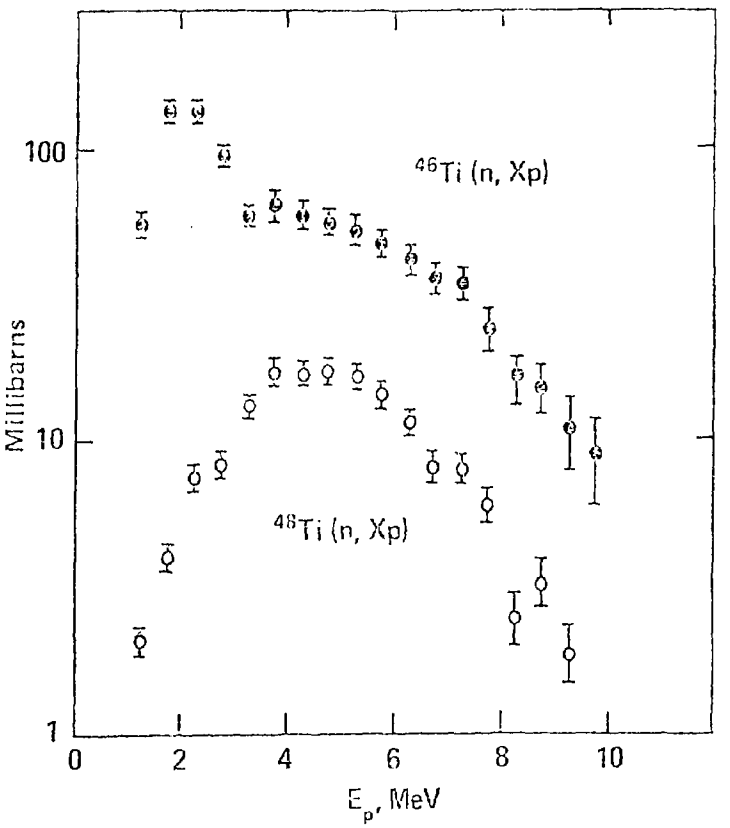

Figure 6

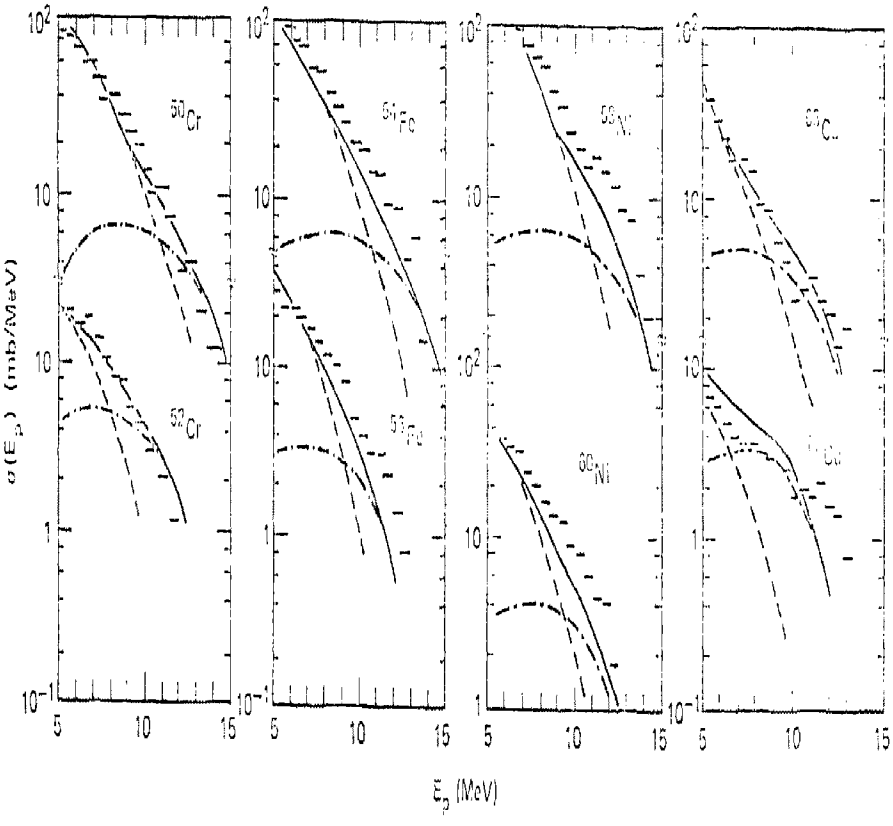
10^2
10
1
10^{-1}
5
10
15
^{50}Cr
^{52}Cr
^{54}Fe
^{56}Fe
^{58}Ni
^{60}Ni
$\sigma(E_p)$ (mb/MeV)
E_p (MeV)

Figure 7

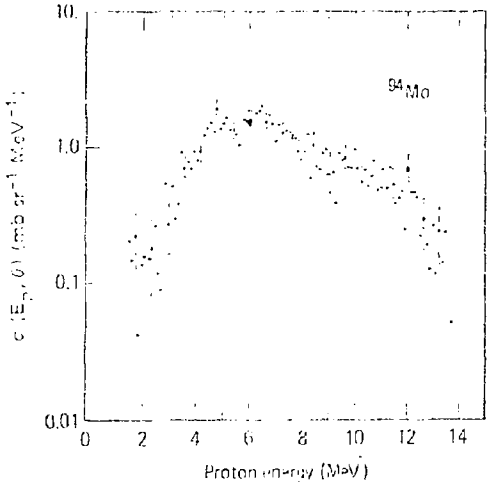

Figure 8